A Simple Model for Surface Charge on Ion Channel Proteins

David Naranjo,* Ramón Latorre,‡ Diana Cherbavaz,*§ Pete McGill,¶ and Mark F. Schumaker¶

*Department of Biochemistry, Brandeis University, Waltham, Massachusetts, USA; ‡Departamento de Biología, Facultad de Ciencias, Universidad de Chile, and Centro de Estudios Científicos de Santiago, Santiago, Chile; and ¶Department of Pure and Applied Mathematics, Washington State University, Pullman, Washington, USA

ABSTRACT We present a simple two-parameter model for surface charge directly associated with ion channels. A spherically symmetric "charged shell" models a distribution of surface charge arrayed about the channel entrance, with a corresponding set of image charges behind the plane of the membrane. The transition between a regime of buffered conductance and a regime of rapidly falling conductance at very low ionic strength is found to depend on the magnitude of the surface charge as well as the separation between the charge and the channel entrance. This resolves an apparent discrepancy between the experimental findings of Naranjo and Latorre (1993. *Biophys. J.* 64:1038–1050) and previous theoretical computations. The charged-shell model is used in a comparative study of the toad skeletal muscle conductance data of Naranjo and Latorre, the rat skeletal muscle conductances of Ravindran et al. (1992. *Biophys. J.* 61:494–508), and a second set of rat muscle conductances presented in this paper.

INTRODUCTION

Surface charge on ion channel proteins may influence their function in several ways. It may enhance conductance by attracting permeant counter-ions (Apell et al., 1977), modulate gating kinetics (Behrens et al., 1989), or influence transitions to subconductance states (Recio-Pinto et al., 1990). More speculatively, negatively charged carbohydrates attached to the extracellular domains of proteins may separate channels via electrostatic repulsion, or they may keep the oligosaccharides themselves in an extended conformation, possibly conferring a reduced autoimmune response or protecting channels from proteases (James and Agnew, 1987). For reviews of surface charge effects in general, see, for example, Green and Andersen (1991) or Latorre et al. (1992). Jordan (1993) has recently provided a broad overview of electrostatic effects on ion channels.

Several sodium channels are known to have surface charges. Miller et al. (1983) and James and Agnew (1987) found carbohydrates linked to the extracellular domain of the *Electrophorus* eel Na^+ channel carrying 110–130 negative charges. More recently, Terlau et al. (1991) found that mutations in two clusters of negatively charged amino acids near the putative permeation pore of rat brain Na^+ channel II reduce both toxin sensitivity and single-channel conductance. Recent experiments measuring the low ionic strength conductance of rat (Ravindran et al., 1992) and toad (Naranjo and Latorre, 1993) Na^+ channels reconstituted in neutral lipid bilayers look for the presence of such charges and provide information related to their structure.

The influence of fixed charges on ion concentrations is often modeled by means of the Poisson-Boltzmann equation. This nonlinear differential equation can be solved analytically for the case of a simple electrolyte bounded by a plane surface with uniform charge density. The result is Gouy-Chapman theory, which has been used to model the electrostatic potential close to a charged bilayer (see, for example, the review by McLaughlin, 1977). Gouy-Chapman theory has been shown to account, qualitatively, for changes in channel properties due to surface charge distributed over lipid bilayers. Examples include an increase in conductance of gramicidin A (Apell et al., 1979), as well as conductance and gating properties of K^+ channels (Bell and Miller, 1984; Moczydlowski et al., 1985). When modeling surface charge effects on large physiological channels, it was found useful to introduce a separation between the charged plane and the channel entrance (Bell and Miller, 1984; Moczydlowski et al., 1985).

However, Gouy-Chapman theory does not accurately reflect the geometry of surface charge associated with an ion channel protein. A fundamental assumption of this theory is that charge is spread over an infinite plane. This makes it difficult to directly interpret charge densities obtained from a Gouy-Chapman analysis of ion channel reconstitution experiments in neutral lipid bilayers.

In order to model charges located close to the ion channel entrance, the Poisson-Boltzmann equation has been solved numerically (Dani, 1986; Cai and Jordan, 1990). Cai and Jordan investigated several different vestibule geometries and possible locations for the fixed charge. They also discussed a "break" that occurs in the conductance, as a function of decreasing permeant ion concentration. When the Debye length exceeds the separation between the channel entrance and the surface charge, they found that the conductance rapidly decreases.

Received for publication 24 May 1993 and in final form 10 September 1993.

Address reprint requests to Dr. Mark F. Schumaker, Department of Pure and Applied Mathematics, Washington State University, Pullman, WA 99164-3113.

§Dr. Cherbavaz's current address is Department of Biochemistry and Biophysics, University of California at San Francisco, San Francisco, California, USA.

0006-3495/94/01/59/12 $2.00

In this paper we introduce a simple surface charge theory with a geometry suitable for modeling charges associated directly with the ion channel protein. The model has only two parameters, the amount of charge and its separation from the channel entrance. These parameters are similar to those used by Gouy-Chapman theory, when a separation between the charged plane and the channel entrance is introduced. Using our new model, we are able to resolve an apparent conflict between the conductance measurements of Naranjo and Latorre and the theoretical analysis of Cai and Jordan. We also present a new set of rat conductance data and apply our new surface charge model in a comparative study of the rat and toad conductances. The results, which have an immediate physical interpretation, are discussed below.

MATERIALS AND METHODS

Rat skeletal muscle preparation

Membranes containing tetrodotoxin (TTX)-sensitive voltage-dependent Na^+ channels were isolated from rat skeletal muscle as described previously (Moczydlowski and Latorre, 1983), with few changes. Initial steps of the procedure were conducted rapidly to the first high-speed spin. Membrane pellets obtained were resuspended by trituration through an 18-gauge needle. The pellet solution (~10% sucrose) was layered on a 28% (w/v) sucrose cushion and spun overnight at 25,000 rpm in an SW28.1 rotor (~18 h). The cloudy band was diluted into a sucrose-free buffer, pelleted (35,000 rpm for 60 min), and resuspended by trituration with a 22-gauge needle mounted on a 1-cc syringe. The material was quickly frozen on dry ice and stored at −70°C. The preparation retained optimal activity for 3–3½ months. Aliquots used daily were maintained on ice during the work day, refrozen (stored at −20°C overnight), and reused.

Solutions and lipid bilayers

Na^+ solutions (between 1 and 10 mM) were prepared from fresh 1 N NaOH standard, 0.1 mM EDTA acid form, dissolved in ddH_2O, and adjusted to pH 7.01 ± 0.03 with solid *n*-morpholino-*p*-sulfonic acid (MOPS) (Sigma, St. Louis, MO). Higher [Na^+] was prepared by the addition of solid NaCl to the base solution (discussed above), and the pH was readjusted by the addition of solid MOPS. Fresh solutions were prepared every other day.

Solutions were continuously stored in a water bath maintained at 25°C during the period the solutions were in use. Measurements were made within 15 min of solution exchange, during which the solution temperature remained constant. Ambient temperature and relative humidity were controlled by heating, dehumidifying, and air conditioning units.

A 7:3 mixture of neutral lipids, 1-palmitoyl-2-oleoly-phosphotidylethanolamine (POPE) and 1-palmitoyl-2-oleoly-phosphotidylcholine (POPC) (Avanti Polar Lipids, Birmingham, AL), was used to cast membranes. Aliquots that were used daily were prepared to a final concentration of 20 mg/ml in *n*-decane (Aldrich Fine Chemicals, Milwaukee, WI) and discarded after use.

Bilayer chambers and membrane formation

To ensure complete exchange of solutions, two-piece home-built compressed Lucite chambers were designed to eliminate any unexchangeable volume. This proved necessary, because the chambers used previously had permitted high-salt solutions (see fusion conditions below) to be trapped in "dead space," that is, a volume of solution unexchangeable by perfusion. After perfusion to low-salt solutions, trapped salt would diffuse into the chamber, increasing the bulk Na concentration.

Planar lipid bilayers were cast upon a hole in a Teflon film (a gift from Alan Finkelstein, Albert Einstein College of Medicine) that was sandwiched between the two halves of the Lucite chamber. Holes with diameters of approximately 150 μm consistently gave good 60–80-pF membranes into which vesicles fused readily. Partitions were spent (became deformed or soiled with lipid residues and dirt) after 3–8 weeks of heavy usage, and the chamber was then rebuilt. The aging of partitions was heralded by an increase in membrane instability. Prior to membrane formation, the Teflon partition was precoated with ~0.25 μl of the lipid solution, and the partition hole was wetted by capillary action. Since membrane stability was critically dependent on complete evaporation of the decane, the lipid was air-dried for 20 min at room temperature. Membranes were cast by a combination of two methods: a lipid bubble blown from the tip of a 1–5-μl microcapillary was passed across the hole, and a fire-polished microcapillary was wetted with lipid and wiped across the hole.

Fusion and experimental conditions

Conditions used to favor vesicle fusion combined an electrochemical gradient with an applied voltage. A typical salt gradient was 100 mM *cis* to 10 mM NaMOPS *trans* at an applied voltage of 50 mV. *cis* was defined as the side of the membrane to which vesicles were added.

After a membrane was formed and determined to be of good quality (that is, the conductance was small, 1–3 pS, and capacitance large), 100 nM batrachotoxin and 5–10 μl of 30–40 μg/ml vesicle preparation (as determined by A280) were added to the solution while stirring. All rat skeletal muscle data collected at pH 7.0 presented below conform to physiological convention (extracellular solution defined as ground).

Because conditions to enhance fusion were different from experimental conditions, both *cis* and *trans* wells were extensively perfused while stirring, using a minimum of 10 chamber volumes. The volume necessary for thorough perfusion was determined from the perfusion of colored dyes and from conductivity measurements. The conductivity of the perfused "experimental" conditions was compared with that of the stock solutions and determined to be identical within error of the measurement after perfusion. Perfusion of the *trans* chamber required shunting the current and voltage passed through the bilayer to prevent membrane damage.

Toxin stocks

Lyophilized batrachotoxon (a generous gift from Dr. John Daly, NIH) was resuspended in 95% ethanol and stored at −70°C. Sodium citrate free crystalline TTX (CalBiochem, LaJolla, CA) was prepared by acidification followed by suspension to a final concentration of 1 mM TTX and 100 mM sodium citrate and stored at −70°C. Daily stocks were stored overnight at −20°C.

Electronics and conductance measurements

Salt bridges of 0.2 M NaCl and 2% bactoagar (Difco, Detroit, MI) were used to electronically connect the $Ag/AgCl_2$ electrodes and experimental solutions. Channel currents were not observed to drift after the new chamber design was introduced. Consistent with this observation, a simple calculation shows that leaching from the salt bridges does not change [Na^+] significantly under the conditions of these measurements.

The voltage clamp circuit utilized a low-noise, high-gain operational amplifier, resulting in an initial gain of 10 mV/pA. Current recordings were filtered at 50 or 100 Hz, which was less than the frequency response of the operational amplifier (~200 Hz). An additional circuit utilizing the current inversion capability of operational amplifiers was added to electronically compensate for transient membrane capacitative changes that occur immediately following a voltage change. This additional circuitry was necessary when acquiring continuous open-channel current-voltage ramps and was turned off at all other times.

All experiments were computer assisted. On-line open-channel current-voltage ramps were computer assisted, stored, and analyzed (Indec, Sunnyvale, CA). The data acquisition and analysis routines were written by Christopher Miller. Each open-current voltage ramp consisted of 64 raw ramps; raw ramps were examined, and subsections of the continuous current

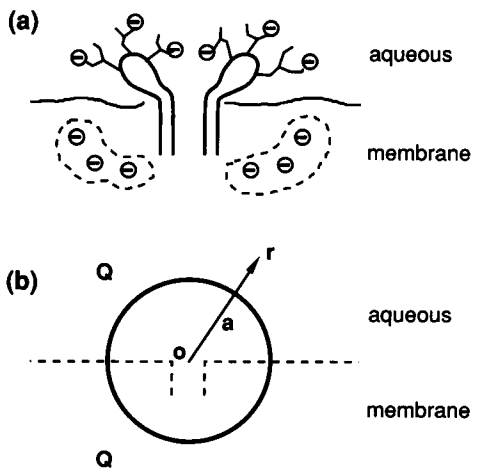

FIGURE 1 Geometry of charges in the charged-shell model. (*a*) Charges associated with the channel protein or attached carbohydrates are assumed to be distributed around and above the channel entrance, which lies in the plane of the membrane. The electric field in the aqueous medium due to polarization at the surface of the membrane is equivalent to that due to a distribution of image charges below the plane of the membrane. (*b*) The charged-shell model assumes that the channel entrance is at the center of a uniform hemisphere of surface charge in the aqueous medium. The hemisphere has radius a and charge Q. A symmetric hemisphere of image charges, also bearing a charge Q, lies below the plane of the membrane.

curve were manually designated as open channel, closed channel, or junk (i.e., transitions between the open and closed states). A measurement was signal averaged before the bare membrane baseline was electronically subtracted, yielding an open-current voltage ramp. Channel conductances, γ_s, were extracted from the slope of such curves.

CHARGED-SHELL MODEL

We describe a very simple, spherically symmetrical model for the influence of surface charge on the electrical potential at the channel entrance. Our use of spherical symmetry is suggested by the calculations of Mathias et al. (1992), who found an analytical solution for the linearized Poisson-Boltzmann equation describing the potential due to a point charge at an infinite interface between a planar membrane (dielectric constant of 2) and a monovalent electrolyte (dielectric constant of 80). In the aqueous hemisphere, they found that the electric field had near-spherical symmetry about the source charge. The symmetry is due to the polarization charges induced at the interface by the electric field of all of the charges in the aqueous medium; the polarization provides a field that is equivalent to one due to a nearly symmetric set of image charges behind the plane of the membrane. The description of the polarization field by the method of images does not depend on the specific distribution of charges in the aqueous medium and remains equally valid when considering the nonlinear Poisson-Boltzmann equation.

Close to the channel molecule, the spherical symmetry will be disrupted by the specific structure of the channel protein. Electrically, the protein and associated carbohydrates comprise a complex structure of charges and multipoles distributed in a heterogeneous dielectric medium, extending both above and below the plane of the membrane. The model we describe below does not attempt to take into account this structure.

We assume that the channel entrance lies at the origin of coordinates and that the entrance is surrounded in the aqueous solution by a uniform hemisphere of surface charge, with radius a and carrying charge Q (see Fig. 1). This hemisphere, the "charged shell," models a collection of charges distributed both around the channel and above the plane of the membrane. These charges may be associated with negative charges on amino acids, such as those recently found near the extracellular mouth of the pore (Terlau et al., 1991), or with carbohydrate groups linked to the extracellular domain of the channel (Miller et al., 1983; James and Agnew, 1987). Below the charged shell, the spherical symmetry is completed by an image hemisphere, also bearing a charge Q.

Mathematically, the charged-shell model corresponds to the Poisson-Boltzmann equation with appropriate boundary conditions in spherical coordinates. The derivation in Appendix A obtains the differential equation

$$\frac{1}{\xi}\frac{d^2}{d\xi^2}\xi\phi = \kappa^2 a^2 \sinh \phi(\xi), \tag{1}$$

with boundary conditions

$$\phi'(0) = 0, \tag{2}$$

$$\lim_{\xi\to\infty} \phi(\xi) = 0, \tag{3}$$

$$\phi(1_+) = \phi(1_-), \tag{4}$$

$$\phi'(1_+) - \phi'(1_-) = s. \tag{5}$$

These equations depend on several dimensionless quantities. The radial coordinate $\xi = r/a$ is the distance to the channel entrance in units of the charged-shell radius a. $\xi = 0$ corresponds to the channel entrance and $\xi = 1$ to the charged shell. The arguments 1_+ and 1_- denote limiting values as the shell is approached from the outside and the inside, respectively. Primes denote derivatives with respect to ξ. The dimensionless electrical potential $\phi(\xi) = e_0\Phi/kT$ is in units of $kT/e_0 \approx 25$ mV, where e_0 is the elementary electrical charge, Φ is the electrical potential, k is Boltzmann's constant, and T is the absolute temperature.

The model depends on two parameters. κa is the ratio of the charged-shell radius a to the Debye length κ^{-1}, and is given by

$$\kappa^2 a^2 = \frac{2e_0^2 c_b a^2}{\epsilon kT} \tag{6}$$

If $T = 293$K, then $\kappa a \approx 3.28\, a c_b^{1/2}$, where a has units of nm and the bulk permeant ion concentration c_b is given in M. The second parameter in the model is the discontinuity in ϕ':

$$s = \frac{e_0}{kT}\frac{|Q|}{2\pi\epsilon a}. \tag{7}$$

s is equal to the magnitude of the unscreened potential of the

charged-shell, divided by about 25 mV. A convenient relation is $s \approx 1.43\ |\zeta|/a$, where ζ denotes the valence of the charged shell, $Q = \zeta e_0$, and a is measured in nanometers.

The charged-shell electrical potential, described by the nonlinear differential equation (Eq. 1) and its boundary conditions, must be computed numerically. However, the very simple way this model depends on the parameters κa and s leads to a physically interesting scaling relationship between solutions. Consider the solution $\phi(\xi)$ associated with a given set of values for a, ζ, and c_b. Now decrease the values of a and ζ by a given factor f: $a \to a/f$, $\zeta \to \zeta/f$. Then s remains fixed and the same value of κa will be recovered if we rescale $c_b \to f^2 c_b$. Since κa and s are the only two parameters in Eqs. 1–5, the same solution $\phi(\xi)$ must be found after rescaling.

The local permeant ion concentration, $c_+(\xi)$, is obtained by application of Boltzmann's principle: $c_+(\xi) = c_b \exp(-\phi(\xi))$. In particular, the concentration at the channel entrance, c_e, which is used to compute conductance, is given by

$$c_e = c_b e^{-\phi(0)} \tag{8}$$

If the quantities a, ζ, and c_b are rescaled as described in the previous paragraph, we would find

$$c_+(\xi) \to f^2 c_+(\xi). \tag{9}$$

That is, if we decrease the radius a and the charge ζ by a common factor f and increase the bulk concentration by a factor f^2, then the same potential $\phi(\xi)$ is obtained, and the local concentration increases everywhere by the same factor f^2.

The charged-shell model may be accurately approximated by linearization when $\phi < 1$; an analytical solution to this problem is given in Appendix B. This linearized problem is closely related to Debye-Hückel theory, which is the solution to the linearized Poisson-Boltzmann equation exterior to a uniformly charged sphere. As we shall see in the next section, the solution of the linearized charged-shell model is closely related to that of the full nonlinear model. However, as discussed in the Appendix, linearization can lead to misleading results, especially when computing concentrations.

NUMERICAL SOLUTION

We solved the full Poisson-Boltzmann equation numerically; some details of the implementation are described in Appendix C. In this section we describe how the electrical potential and resultant local ion concentrations depend on the radius and valence of the charged-shell and the bulk ion concentration.

Fig. 2 *A* shows how the potential, ϕ, depends on distance from the channel entrance, ξ, for a charged shell of radius $a = 5$ nm, valence $\zeta = -20$, and for several values of bulk concentration, c_b. Numerical solutions of the nonlinear model Eq. 1 (solid curves) are compared with the analytical solution, Eq. 18 in Appendix B, of the linearized equations (dashed curves). The channel entrance, at $\xi = 0$, corresponds

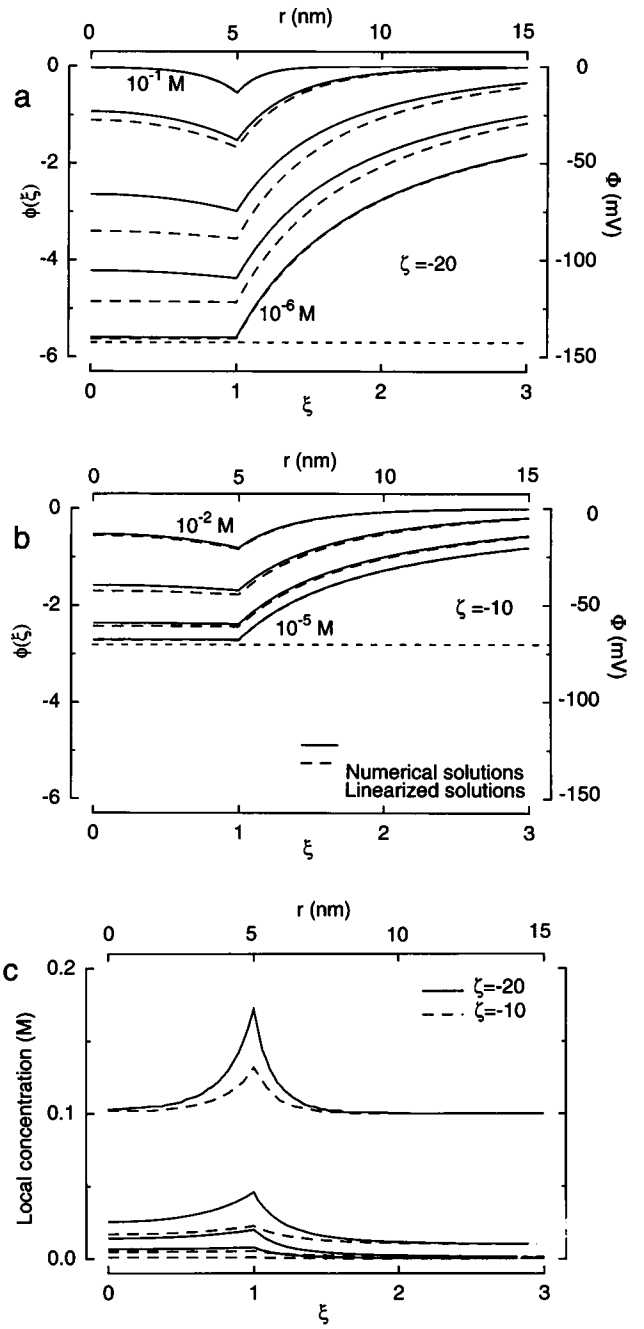

FIGURE 2 Electrical potential ϕ and counter-ion concentrations as a function of distance ξ from the channel entrance. ϕ is measured in units of $kT/e_0 \approx 25$ mV, and ξ is measured in units of the shell radius a. (*a*) Potentials for $a = 5$ nm and $\zeta = -20$. Five pairs of curves are shown, corresponding to $c_b = 10^{-1}, 10^{-2}, 10^{-3}, 10^{-4}$, and 10^{-6} M, in order of decreasing potentials. Solid curves show ϕ computed numerically for the full charged-shell model, Eq. 1, and dashed curves show the solution of the linearized theory, Eq. 18. Solutions for $c_b = 10^{-1}$ M cannot be distinguished. The dotted line across the bottom of the figure indicates the unscreened potential $-s = -5.72$. (*b*) Potentials for $a = 5$ nm and $\zeta = -10$. Four pairs of curves are shown, corresponding to $c_b = 10^{-2}, 10^{-3}, 10^{-4}$, and 10^{-5} M. The dotted line indicates $-s = -2.86$. (*c*) Counter-ion concentrations for $c_b = 10^{-1}, 10^{-2}, 10^{-3}$, and 10^{-4} M. Solid curves correspond to $a = 5$ nm and $\zeta = -20$, and dashed curves correspond to $a = 5$ nm and $\zeta = -10$.

to the left-hand margin of the figure. The charged shell is located at $\xi = r/a = 1$. Its surface charge density results in a discontinuity in the slope of the potential (Eq. 5). The values $a = 5$ nm and $\zeta = -20$ correspond to a charge density of about $1e_0$ per 8 nm^2, computed using the surface area of the hemisphere.

When $c_b = 0.1$ M, near physiological ionic strength, counter-ions strongly screen the charged shell and $|\phi(\xi)| < 1$. As a consequence, the solution of the linearized equation approximates the behavior of the full model very well. ϕ is only appreciably different from zero in the immediate vicinity of the shell, and there is no significant enhancement of ion concentration at the channel entrance, $c_e \approx c_b$. The clustering of counter-ions near the charged shell can also be seen in Fig. 2 *C*. We refer to this high-ionic-strength scenario as the "strongly screened regime."

At the lowest bulk ion concentration shown, $c_b = 10^{-6}$ M, there is practically no screening. Values of ϕ inside the charged shell are nearly constant, and their magnitudes approach an unscreened limit of $s = 5.72$, which is simply the solution for a charged sphere in a dielectric medium. Then $c_e \approx c_b e^s$. We refer to this low-ionic-strength scenario as the "weakly screened regime."

At the intermediate values of c_b there is a significant gap between the solution of the linearized model and the numerical results. Magnitudes of the numerically computed potentials are always less than those given by the linearized solution because the linearization $\sinh \phi \rightarrow \phi$ underestimates the screening. As c_b decreases in this regime, values of c_e are enhanced because the potential $\phi(0)$ becomes increasingly negative as the screening grows weaker (see Eq. 8). For example, as c_b decreases 100-fold, from 10 mM to 0.1 mM in Fig. 2 *C*, c_e decreases only 4-fold, from 25.3 to 6.9 mM. We therefore call this intermediate-ionic-strength scenario the "buffered regime."

Fig. 2 *B* shows how potentials change when the magnitude of the surface charge decreases by a factor of 2. In this example $a = 5$ nm and $\zeta = -10$. As c_b decreases to zero, the magnitude of the potential approaches an unscreened limit of $s = 2.86$. As compared with the previous example, a significant gap between the solution of the linearized model and the numerical results appears over a narrower intermediate range of c_b. Corresponding concentrations are given as dashed lines in Fig. 2 *C*.

The solutions shown in Fig. 2 will also apply when parameters and concentrations are appropriately rescaled, as described below Eq. 9. For example, divide both a and ζ in Fig. 2 *A* by the factor $f = 5$ to consider a model with charged-shell radius $a = 1$ nm and valence $\zeta = -4$. After multiplying c_b by $f^2 = 25$, the dimensionless parameters κa and s remain unchanged, and the same solution $\phi(\xi)$ of Eq. 1 must be obtained. The five pairs of curves shown in Fig. 2 *A* are recovered, with the top pair now corresponding to $c_b = 2.5$ M and the bottom pair corresponding to $c_b = 2.5 \times 10^{-5}$ M. Concentrations shown on the ordinate of Fig. 2 *C* must also be multiplied by a factor of 25 to give corresponding values of $c(\xi)$. This example suggests that two possible sources of surface charges, charged amino acid residues within a nanometer of the channel entrance versus charged sialic acids perhaps 5–10 nm from the channel entrance, would lead to easily distinguished effects, since they will involve much different concentration ranges.

Fig. 3 shows how $\log_{10} c_e$ varies as a function of $\log_{10} c_b$. Three triplets of curves are shown, corresponding to $s = 2.86$, 5.72, and 8.58. The three curves within each triplet merge into a common line with slope 1 at very low c_b. The slope reflects the linear proportionality $c_e \approx c_b e^s$ in the weakly screened regime. A formula for the limiting tangent line, as $c_b \rightarrow 0$, is given by taking logarithms:

$$\log_{10} c_e \approx 0.4343s + \log_{10} c_b. \qquad (10)$$

Therefore, s is reflected in Fig. 3 by the intercept of this tangent line. For an ion channel embedded in a neutral lipid bilayer, any localized distribution of charges, separated from the channel entrance, will also give $c_e \rightarrow 0$ as $c_b \rightarrow 0$, similar to the charged-shell model. This low-ionic-strength behavior of the charged-shell model is qualitatively different from that of Gouy-Chapman theory, where a nonzero residual counterion concentration at the membrane surface remains as $c_b \rightarrow 0$.

At sufficiently high c_b the surface charges are heavily screened, and the channel entrance falls outside of their influence. This was shown by Fig. 2. Then $c_e \approx c_b$ and the curve of entrance concentrations again approach a limiting slope of 1, as seen near the right-hand margin of Fig. 3.

The buffered regime spans intermediate concentrations and is particularly pronounced when s is large. If, in addition, a is also large, screening effects due to counter-ions become important at low c_b. Then the conductance, if it is proportional to c_e, may be significant and only weakly dependent on c_b at the lowest observable concentrations.

The scaling relationship is especially simple in logarithmic coordinates. Letting $a \rightarrow a/f$ and $\zeta \rightarrow \zeta/f$, the same ϕ is obtained by rescaling $c_b \rightarrow f^2 c_b$ and $c_e \rightarrow f^2 c_e$. The resultant

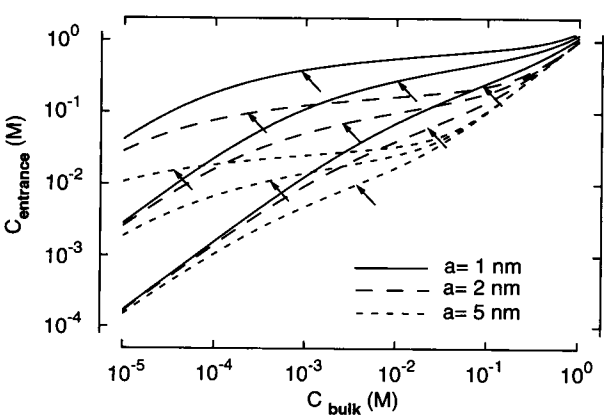

FIGURE 3 Entrance concentration c_e as a function of bulk concentration c_b. Axes are logarithmically scaled. Arrows point out neutralization concentrations. Solid curves correspond to $a = 1$ nm and $\zeta = -2$, -4, and -6; dashed curves to $a = 2$ nm and $\zeta = -4$, -8, and -12; and dotted curves to $a = 5$ nm and $\zeta = -10$, -20, and -30.

solutions in Fig. 3, corresponding to different values of a but fixed values of s, are "rigidly" translated, parallel to lines with slope 1.

NEUTRALIZATION CONCENTRATION

Naranjo and Latorre (1992) found that the conductance γ of reconstituted toad Na^+ channel in neutral lipid bilayers depends on bulk $[Na^+]$ only weakly at concentrations as low as 0.4 mM. They proposed that surface charges enhance conductance at low ionic strength. Cai and Jordan (1990) have carried out a numerical study of the influence of surface charges localized on the vestibules of ion channels under conditions of low ionic strength. They concluded that, as ionic strength decreases, conductance begins to drop rapidly when the Debye length in the electrolyte exceeds the separation between the surface charges and the channel entrance.

This conclusion of Cai and Jordan appears to conflict with the explanation of Naranjo and Latorre. Below $[Na^+] = 1$ mM, the Debye length is greater than 10 nm. However, the Stoke's radius of the $[Na^+]$ channel is only 9.5 nm (Agnew et al., 1978), and surface charges localized to the channel protein could hardly be located much farther than this from the channel entrance. The conclusion of Cai and Jordan then suggests that, if toad $[Na^+]$ channel conductances were enhanced by surface charges, their conductance should be dropping rapidly to zero once the ionic strength was as low as 1 mM. This apparent contradiction motivates us to characterize the transition between the buffered and weakly screened regimes of the charged-shell model.

We take a simple approach. In the absence of counter-ions, the charged-shell model leads to the problem of a uniformly charged sphere in a dielectric medium. The potential inside the sphere has the constant value $-s$. When c_b is vanishingly small, the counter-ion concentration inside the sphere is therefore constant and equal to $c_b e^s$. Suppose we assume this relationship holds at finite bulk concentrations. For what value of c_b would the accumulated counter-ion charge inside the shell neutralize the fixed charge Q on the shell? We call this the "neutralization concentration," c_n.

We will show that c_n gives a practical upper bound for the value of c_b at the transition from the weakly screened regime to the buffered regime. Note that the weakly screened regime approximates the unscreened limit. The potential at the channel entrance $\phi(0) \approx -s$ and is nearly uniform inside the charged shell. The counter-ion concentration inside the shell is therefore nearly constant and given by $c_e \approx c_b e^s$. For values of s of practical interest, in the weakly screened regime, we may neglect the contribution that co-ions make to the total charge inside the shell. For example, if $s > 2.3$, then the counter-ion concentration is approximately $c_b e^s > 10\, c_b$, and the co-ion concentration is approximately $c_b e^{-s} < 0.1\, c_b$.

Now let $c_b = c_n$, $s > 2.3$, and suppose the system is in the weakly screened regime. We would then have $c_e \approx c_n e^s \gg c_n = c_b$. But then, by the definition of the c_n, the positive charge carried by the counter-ions is greater in magnitude than the negative surface charge distributed on the shell. This would imply that the net charge of the shell and its contents is positive, so that $\phi(0) > 0$. The original assumption that $\phi(0) \approx -s$ thus leads to a contradiction, showing that the system cannot be in the weakly screened regime.

To calculate c_n, set $Q + Q_n = 0$, where $Q = \zeta e_0$ and Q_n is the charge carried by counter-ions inside the shell. Neglecting screening, and setting $c_b = c_n$, we obtain $Q_n = (2\pi a^3/3) c_n e^s e_0$. Solving for c_n, we obtain

$$c_n \approx 0.793 \frac{|\zeta|}{a^3} e^{-s} \approx 0.556 \frac{s}{a^2} e^{-s}, \qquad (11)$$

where a is measured in nanometers and values of c_n obtained have units of molarity. Values of the neutralization concentrations are shown by the arrows in Fig. 3. Note that under the scaling $a \to a/f$ and $\zeta \to \zeta/f$, with s fixed, we obtain $c_n \to f^2 c_n$, consistent with the scaling of c_b.

We next apply the criterion of Cai and Jordan to the charged-shell model and compare it with the upper bound estimated by c_n. Recall that κa is the ratio of the charged-shell radius a to the Debye length and assume that the conductance is proportional to c_e at low ionic strength. Then the criterion estimates that the conductance will begin to drop rapidly, as a function of decreasing ionic strength, when κa decreases below 1. For the charged-shell geometry, this corresponds to estimating that the transition between the weakly screened and buffered regimes takes place at a value of $c_b = c'$ for which $\kappa a = 1$. Then $c' \approx 0.0930/a^2$, with a measured in nanometers and c' in molarity.

How does c' compare with c_n? Note first that c' is independent of s. From the last expression in Eq. 11, one finds $c_n > c'$ for $0.20 < s < 2.83$ and $c' > c_n$ otherwise. For example, in Fig. 3, c' very nearly agrees with values of c_n when $s = 2.86$. Note that c' does satisfy the scaling relation described below Eq. 9; letting $a \to a/f$ we obtain $c' \to f^2 c'$. Therefore, regardless of a, for $s < 2.86$, c' may provide a good estimate of the transition between the weakly screened and buffered regimes. However, for much larger values of s, c' substantially overestimates the value of c_b at this transition. For example, when $a = 5$ nm and $\zeta = -20$, giving $s = 5.72$, we have $c' \approx 3.6$ mM and $c_n \approx 0.4$ mM.

This comparison of c_n and c' explains the discrepancy between the conductance measurements of Naranjo and Latorre and the estimate of Cai and Jordan. If surface charges are present and $s \gg 2.8$, a weak dependence of conductance on bulk permeant ion concentration can persist even though the Debye length is greater than the separation between the charges and the channel entrance.

ANALYSIS OF CONDUCTANCE DATA

This study was motivated by recently measured conductances of $[Na^+]$ channels at very low ionic strength (Cherbavaz, 1991; Ravindran et al., 1992; Naranjo and Latorre, 1993). These measurements are very sensitive to surface charge effects. Since the channels are reconstituted in neutral lipid bilayers, any surface charges must be directly associated with the ion channel. Naranjo and Latorre, study-

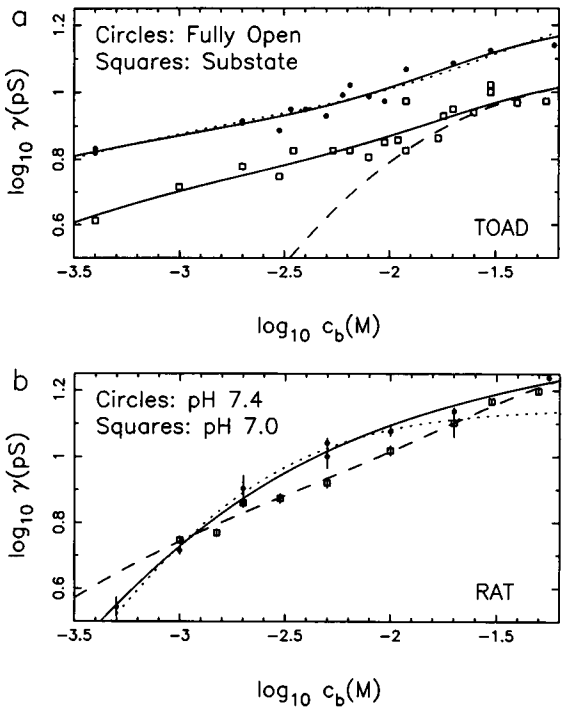

FIGURE 4 Charged-shell analysis of toad and rat Na^+ channel conductances. (*a*) Toad conductances. Circles show measured fully open state conductances and squares show measured substate conductances. The upper solid line shows the L/CS model fit to fully open data corresponding to K_C = 9.15 mM, and the dotted line shows the fit corresponding to K_C = 17.7 mM. The lower solid line shows the K_C = 9.15 mM L/CS fit to substate conductances, and the dashed line indicates the Langmuir isotherm corresponding to the same values of γ_{max} and K_C, but without surface charge effects. (*b*) Rat conductances. Circles show the pH 7.4 conductance measurements of Ravindran et al. (1992), and squares show the pH 7.0 measurements presented in this paper. The solid line shows the K_C = 17.7 mM L/CS fit to the pH 7.4 data. The dotted line is the best fit Langmuir isotherm to the c_b < 20 mM portion of this data, optimized parameters are γ_{max} = 14.0 pS, and K_C = 1.60 mM, without surface charge. Finally, the dashed line shows the K_C = 17.7 mM L/CS fit to the pH 7.0 data.

ing Na^+ channels from toad skeletal muscle, found that a weak dependence of conductance on ion concentration persisted down to concentrations as low as 0.4 mM. They explained these results as being due to surface charges enhancing local ion concentration near the channel entrance. However, Ravindran et al., studying Na^+ channels from rat skeletal muscle at pH 7.4, concluded that their data could be explained without surface charges. The data published in this paper (Cherbavaz, 1991) are also conductance measurements from rat skeletal muscle Na^+ channels. The experimental protocol is similar to that of Ravindran et al.; however, the experiments were performed at pH 7.0. All of these data are presented in Fig. 4. In this section, we analyze them using the charged-shell model.

The charged-shell model gives values of c_e as a function of c_b. A dependence of the conductance γ on c_e must also be introduced. Although there is evidence for multiple occupancy at high ionic strength (Correa et al., 1991; Ravindran et al., 1992; Naranjo and Latorre, 1993), we assume that, at the low Na^+ concentrations of concern here, multiple occupancy is unimportant. One can then use the general theoretical result (Läuger, 1973; Levitt, 1986) that γ depends on c_e according to a Langmuir isotherm expression:

$$\gamma = \frac{\gamma_{max} c_e}{K_C + c_e}, \tag{12}$$

where K_C is an effective dissociation constant of the ion from the channel and γ_{max} is the saturation value of the conductance. Our use of the Langmuir formula also follows the analysis of Cai and Jordan (1990). Although the present discussion is set in the context of rate theory models, we emphasize that Eq. 12 also applies to single-ion diffusion models (Levitt, 1986). We call this combination of the Langmuir isotherm with surface charge effects the L/CS model.

Both Ravindran et al. (1992) and Naranjo and Latorre (1993) analyzed their data in terms of symmetrical or nearly symmetrical 3B2S models. Dissociation constants may be deduced from the model binding site energies. As discussed in Appendix D, what one obtains directly from these energies is the dissociation constant $K_S = \exp(-E_{site}/kT)$ for a binding site, where E_{site} is the energy of an ion bound at a binding site relative to a standard aqueous solution. For a symmetrical 3B2S channel, $K_C = K_S/2$. The $-4.0kT$ energy wells (1 M standard state) of the Naranjo and Latorre model correspond to K_C = 9.15 mM. The $-9.6kT$ energy wells (55.5 M standard state) of the Ravindran et al. model correspond to K_C = 1.85 mM. Cherbavaz (1991) fit her data directly with a Langmuir conductance model using Gouy-Chapman surface charge effects and found the optimized value K_C = 17.7 mM.

We have analyzed all of the data sets in Fig. 4 using K_C = 1.85, 9.15, and 17.7 mM. Results for 9.15 and 17.7 mM are given in Table 1. Fits were made only to data for c_b < 60 mM, shown in Fig. 4. Values of K_C were fixed, and γ_{max}, a, and ζ were optimized without constraint using the nonlinear least-squares algorithm of Neader and Mead (Press et al., 1986). Logarithms of conductances values were used in the optimization. In each case shown in Table 1, essentially identical results were obtained using three widely separated sets of initial parameter values.

TABLE 1 L/CS analysis of Na^+ channel conductances

	Toad fully open	Toad substate	Rat pH 7.0	Rat pH 7.4
K_C (mM)	9.15	9.15	9.15	9.15
γ_{max} (pS)	16.8	11.8	18.5	19.0
a (nm)	8.29	7.19	9.29	3.66
ζ	-36.3	-25.0	-27.2	-4.9
RMS error*	5.5%	8.8%	3.7%	4.6%
s	6.3	5.0	4.2	1.9
K_C (mM)	17.7	17.7	17.7	17.7
γ_{max} (pS)	19.2	13.5	21.7	20.6
a (nm)	6.18	5.51	6.21	2.61
ζ	-26.7	-20.0	-17.1	-4.52
RMS error	6.1%	8.9%	3.7%	4.4%
s	6.2	5.2	3.9	2.5

* The logarithmic RMS error × 100. This is approximately equal to the RMS relative error, $(\gamma_i - \bar{\gamma}_i)/\bar{\gamma}_i$, expressed as a percentage. Here, γ_i is a measured conductance and $\bar{\gamma}_i$ is the model conductance at the same c_b.

Fig. 4 *A* shows fully open state and substate Na^+ channel conductances measured by Naranjo and Latorre (1993). Individual conductance measurements are shown; their scatter indicates the measurement error. The solid curves show the optimal K_C = 9.15 mM L/CS analysis. The dashed curve approaching the substate solid curve shows a Langmuir isotherm with the same γ_{max} and K_C, but without surface charge effects. This relationship is typical; the surface charge distributions shown in Table 1 only lead to a significant enhancement of conductances for c_b < 20 mM. The dotted curve shows the optimal K_C = 17.7 mM fully open conductance. Both values of the dissociation constant lead to attractive fits. Clearly, the low-ionic-strength data do not uniquely specify all four parameters of the L/CS model; one value must be specified from outside the analysis. Nevertheless, optimized values for the surface charge parameters shown in Table 1 are generally consistent. They suggest that 20–40 negative charges are distributed 5–9 nm from the channel entrance.

Optimization using K_C = 1.85 nm was also performed; these analyses are not shown. They lead to charged-shell radius values of a = 24.1 and 16.6 nm for the fully open and substate data, respectively. These values are significantly greater than the 9.5 nm Stokes radius of the Na^+ channel (Agnew et al., 1978). Their RMS errors of 7.1% and 10.8%, respectively, are also considerably greater than those shown in Table 1.

Fig. 4 *B* shows the two sets of rat skeletal muscle conductances measured by Ravindran et al. (pH 7.4) and Cherbavaz (pH 7.0). Both of these data sets show averaged measurements at each c_b, and error bars indicate the SEM. The optimal L/CS fits using K_C = 17.7 mM are shown by the solid (pH 7.4) and dashed (pH 7.0) curves. Fits using K_C = 9.15 mM (not shown) also interpolate the c_b < 60 mM data very well. Corresponding parameter values are given in Table 1. The small RMS errors of these analyses, as compared with those for the toad data, reflect that fact that the rat data are averaged values. The L/CS analysis of the pH 7.4 data indicates the presence of many fewer charges than the analysis of the toad data, as is also reflected by the much smaller values computed for s. Surface charge parameters obtained from the pH 7.0 rat data are generally consistent with the toad results but suggest somewhat smaller values of s.

We also attempted to fit both rat data sets using the L/CS model, using K_C = 1.85 mM. Poor results were obtained. Values of a greatly exceeded the Stokes radius, RMS errors were much larger than in Table 1, and fits from duplicate initial conditions either did not converge at all or converged to different optimal values. These results are not surprising. If the Langmuir part of the model is already designed to interpolate the conductance measurements at lowest ionic strength, then we would expect a vanishingly small optimal surface charge, and the charged-shell radius a will not be sensibly specified by the data. A good fit to the pH 7.0 conductance data for c_b < 20 mM is shown in Fig. 4 *B* using a Langmuir model without surface charge. This fit corresponds closely to the conductance obtained from the 3B2S model by Ravindran et al., when constrained to single ion occupancy.

DISCUSSION OF DATA ANALYSIS

The L/CS analysis of toad conductances suggests that 20–40 charges are distributed 5–9 nm away from the channel entrance. The analysis of the pH 7.0 rat data is similar, except that ζ, reflecting the charge-to-radius ratio, is smaller. In contrast to this, the analysis of the pH 7.4 data of Ravindran et al. finds comparatively few charges. This apparent variation in the importance of surface charges parallels the conclusions of previous studies. Naranjo and Latorre (1993) analyzed the toad conductance data using a 3B2S permeation model with double occupancy and Gouy-Chapman theory for surface charge. They found an intracellular charge density of 0.022 e_0 nm^{-2} and an extracellular density of 0.041 e_0 nm^{-2}. Cherbavaz (1991) has analyzed the pH 7.0 rat data using a Langmuir/Gouy-Chapman model and found an (implicitly symmetrical) charge density of 0.026 e_0 nm^{-2}. Ravindran et al. (1992) concluded that their results could be explained without surface charge effects.

Although the L/CS model reaches the same conclusions regarding the apparent importance of surface charges as the previous modeling studies, its more realistic geometry makes the physical implications of these results clearer. The toad analysis is consistent with charges carried by ionized sialic acid residues on oligosaccharide chains attached to the channel protein (Miller et al., 1983; James and Agnew, 1987). Neuraminidase treatment at physiological ionic strength does not change the magnitude of open channel conductance (Scheuer et al., 1988). However, these findings do not contradict the sialic acid hypothesis; the charged-shell model predicts an appreciable surface charge enhancement of conductance only for c_b < 20 mM. The L/CS analysis of toad conductances is probably not compatible with surface charge effects due to amino acid residues close to the channel entrance, such as those found by Terlau et al. (1991). As described under Numerical Solution above, such charges would rescale conductance features, such as the onset of the weakly screened regime, to much higher ionic strengths.

Our analysis of the rat data at pH 7.0 may be compared with the preliminary observations of Jordan (1993), who analyzed the data of Cherbavaz by solving the Poisson-Boltzmann equation for a collection of discrete charges around a channel entrance. A good fit was obtained with 20 charges arranged 3.5–4.5 nm from the entrance. While this finding is broadly compatible with the L/CS analysis, it does suggest a significantly smaller separation between the charges and the channel entrance. A key difference between the modeling methodologies may be that Jordan analyzed the whole conductance data set, while we have confined ourselves to data taken for c_b < 60 mM.

There is a small difference between the shapes of the pH 7.0 and pH 7.4 conductance curves. The error bars shown in Fig. 4 *B* are only one standard deviation of the mean, and the differences between the individual pH 7.0 and pH 7.4 data

points are at most marginally significant. Yet, taken as a whole, the discrepancy appears systematic. It leads to different conclusions in the L/CS analysis, paralleling the findings of previous studies.

COMPARISON WITH DISCRETE CHARGE MODELS

The charged-shell model assumes that charge is distributed uniformly over a sphere (including both the hemispherical shell and its image) surrounding the channel entrance. In reality, charges are discrete. In this section, we compare entrance concentrations calculated for the charged-shell model with those due to discrete distributions of charges.

The nonlinear Poisson-Boltzmann equation was solved in three dimensions by the program DELPHI (see, for example, Nicholls and Honig, 1991). The channel entrance was placed at the center of a 65 × 65 × 65 rectangular lattice. Solutions were first computed for a lattice length that concentrated all fixed charges near the center of the lattice and assigned a potential $\phi = 0$ to the lattice boundaries. These preliminary solutions were then used to assign boundary conditions to rescaled problems. The lattice length scale was decreased over two iterations until the fixed charge structure filled approximately 80% of the lattice volume. Fixed charges were centered on the surface of spheres circumscribed around the channel entrance. Configurations of eight charges were distributed on the vertices of a cube, and those of 20 charges were distributed on the vertices of a dodecahedron. Note that these configurations are constructed so that, in the linear limit of no screening counterions, they give the same potential at the channel entrance as the spherical shell.

Fig. 5 *A* shows the results of locating the fixed charges 5 nm from the channel entrance. Entrance concentrations computed from the charged-shell model are generally very close to those of the discrete distributions. The only exceptions are the two calculations involving single fixed charges, where c_e was found to be significantly less than when computed by the charged-shell model. This difference may be the result of high counter-ion concentrations close to the fixed charge, due to the nonlinear screening term in Eq. 1.

Fig. 5 *B* shows the results of locating the fixed charges 1 nm from the entrance. Entrance concentrations computed for the single fixed charges are again less than those given by the charged-shell model, but now some values of c_e computed from distributions of 8 and 20 discrete charges are significantly greater than those the charged-shell gives. A possible explanation for this upward deviation lies with the finite radius of the discrete charges, which forces the first screening layer of counter-ions to within 6 Å of the channel entrance.

The charged-shell model is a type of "smeared-charge" approximation and is, in this respect, analogous to Gouy-Chapman theory. Our results are reminiscent of calculations which suggest that Gouy-Chapman theory may accurately approximate the screening of a lattice of fixed, monovalent charges by monovalent counter-ions. In the linear approximation, Gouy-Chapman theory is accurate when the lattice

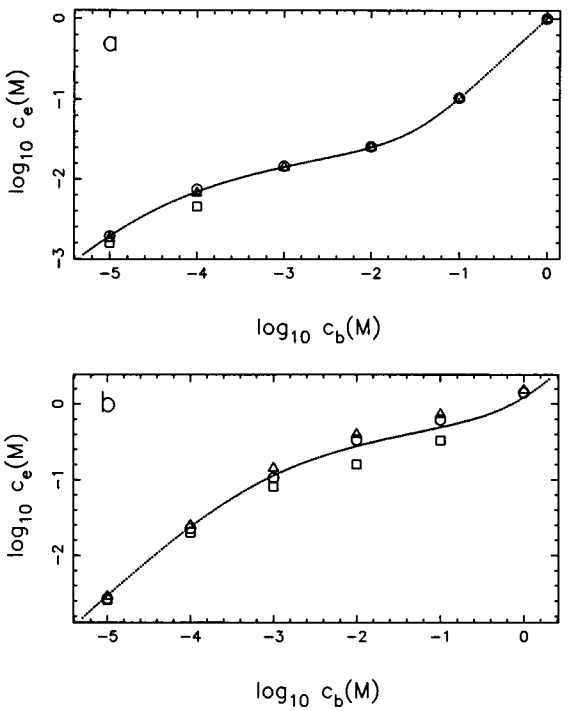

FIGURE 5 Comparison of charged-shell model with discrete charge distributions. Identical discrete charges are centered on spheres of radius a and bear a total charge of valence 2ζ. Entrance concentrations are calculated from potentials computed by DELPHI in each configuration. Symbols represent results from different discrete charge configurations. Dotted lines represent c_e computed from the charged-shell model. Each dot represents a separate calculation. (*a*) a = 5 nm and $\zeta = -20$. Configurations include: □, one charge of radius 2 nm; ○, eight charges of radius 1 nm; △, 20 charges of radius 4 Å. (*b*) a = 1 nm and $\zeta = -4$. Configurations include: □, one charge of radius 4 Å; ○, eight charges of radius 4 Å; △, 20 charges of radius 4 Å.

spacing is comparable to or less than the Debye length and, in addition, counter-ions cannot approach the fixed charges more closely than a Debye length (Nelson and McQuarrie, 1975). Interestingly, experiments have failed to find discreteness-of-charge effects in charged lipid bilayers (Hartsel and Cafiso, 1986; Winiski et al., 1986).

SUMMARY

Ion channel reconstitution experiments in neutral lipid bilayers and at low ionic strength explore the properties of surface charge near the channel entrance. In this paper we present a new set of rat skeletal muscle Na^+ channel conductance data and undertake a comparative study of surface charges near the channel entrance. This study is aided by a new model for surface charges associated with ion channels.

The new model is very simple. The channel entrance is envisioned to lie in the plane of the membrane, centered within a uniform hemisphere of charges in the aqueous solution, and with a hemisphere of image charges below the entrance completing the spherical symmetry. There are only two parameters, the total charge $Q = e_0 \zeta$ of the hemispherical charged shell and the separation a between this charge and the channel entrance.

The charged-shell model, based on the nonlinear Poisson-Boltzmann equation, must be solved numerically. However, we have a global picture of the solutions, as shown by Fig. 3. At very low ionic strength, when screening is unimportant, the entrance concentration is given by $c_e \approx c_b e^s$, where c_b is the bulk ion concentration and $s \propto |Q|/a$ is the magnitude of the unscreened potential at the channel entrance. At very high ionic strength $c_e \approx c_b$, since the entrance is effectively screened from the charge. At intermediate ionic strength there is a regime of "buffered" entrance concentrations, within which c_e is a sublinear function of c_b. The conductance may then be only weakly dependent on bulk permeant ion concentration.

The charged-shell model also has simple analytical properties, which can help reveal important features of surface charge. This differential equation for the charged-shell model, together with its boundary conditions, has a simple scaling property: replacing $a \to a/f$ and $\zeta \to \zeta/f$ one obtains geometrically similar solutions in the rescaled permeant ion concentrations $c_+(\xi) \to f^2 c_+(\xi)$. Scaling arguments can help choose between charge models involving very different charges or characteristic distances between the charges and the channel entrance. For the three sets of conductance data (two toad and one rat), which appear to exhibit important surface charge effects, scaling suggests that these effects are not due to a small number of charges located within a nanometer of the channel entrance.

We have also found a simple upper bound for the bulk permeant ion concentration at the transition between the weakly screened and buffered regimes. This upper bound is called the neutralization concentration. Although the very weak dependence of conductance on ionic strength found by Naranjo and Latorre (1993) appears to conflict with a theoretical finding of Cai and Jordan (1990), we used the neutralization concentration to show that the observations are consistent with theory if the magnitude of the unscreened potential at the channel entrance is sufficiently high.

The charged-shell theory combined with a Langmuir isotherm model of conductance at low ionic strength was used to analyze a new set of rat Na^+ channel conductance data presented in this paper, as well as the previously published rat Na^+ channel conductances of Ravindran et al. (1992) and toad Na^+ channel conductances of Naranjo and Latorre (1993). Good fits were obtained to all data sets. However, the Langmuir dissociation constant is not uniquely specified by the low-ionic-strength data and must be fixed by other considerations.

The fits to the toad data indicate the presence of 20–40 negative charges distributed 5–9 nm from the channel entrance. These results are consistent with surface charges associated with acidic groups on the carbohydrate coat. The electrical influence of such charges on ion permeation will only become appreciable at low ionic strength, below about $c_b = 20$ mM.

The fits to the rat conductance data presented in this paper, taken at pH 7.0, are generally consistent with the toad results but point to a somewhat smaller value of s. In contrast, the analysis of the conductance data of Ravindran et al. (1992), taken at pH 7.4, is consistent with their earlier conclusion, namely that surface charges are not important for this channel. The divergent conclusions arrived at concerning surface charges on the rat Na^+ channels are reflected in previous analyses of the same data (Cherbavaz, 1991; Ravindran et al., 1992). They are based on small but apparently systematic differences between the two sets of conductances at low ionic strength. We have not explained this discrepancy.

APPENDIXES

A. Poisson-Boltzmann equation for the charged-shell model

This appendix develops the Poisson-Boltzmann equation for the charged-shell geometry. Poisson's equation describes the electric field due to a distribution of charges. In MKS units:

$$\nabla^2\Phi = -\frac{\rho}{\epsilon}, \tag{13}$$

where Φ is the electric potential, ρ the charge density, and $\epsilon = \epsilon_a\epsilon_0$ is the product of the dielectric constant of the aqueous solution ϵ_a and the permittivity of free space ϵ_0. Assuming a monovalent electrolyte, the charge density is given by

$$\rho = e_0c_+ - e_0c_- = -2e_0c_b \sinh \phi. \tag{14}$$

Here c_+ and c_- signify the local concentrations of positive and negative ions, respectively. They are related to their concentration in the bulk solution c_b by Boltzmann factors: $c_+ = c_be^{-\Phi}$ and $c_- = c_be^{\Phi}$, where $\phi = e_0\Phi/kT$ is the dimensionless electrical potential, k is Boltzmann's constant, and T is the absolute temperature. Substituting Eq. 14 into Eq. 13, we obtain the Poisson-Boltzmann equation.

Boundary conditions may be developed by initially considering the problems inside and outside the shell separately. Since the Poisson-Boltzmann equation is of second order, we specify two boundary conditions for each. At the origin of coordinates, the electric field is zero, by spherical symmetry. Letting r be the radial variable in spherical coordinates, the interior problem therefore satisfies $E_r(r = 0) = -(\partial\Phi/\partial r)_{r=0} = 0$. As $r \to \infty$, the potential decays to a constant value, taken to be 0. This gives a condition for the exterior problem: $\lim_{r\to\infty} \Phi = 0$.

The two remaining boundary conditions are found at the shell, where the problems join. First, the potential is itself continuous at the shell: $\Phi(a_+) = \Phi(a_-)$. Here, $\Phi(a_+)$ denotes the limiting value of the potential as r approaches a from more positive values, and $\Phi(a_-)$ denotes the corresponding limit as r approaches a from more negative values. The second boundary condition is obtained by applying Gauss' law at $r = a$. There we find a discontinuity in the derivative of the potential due to the surface charge:

$$E_r(a_+) - E_r(a_-) = \frac{\sigma}{\epsilon} = \frac{Q}{2\pi a^2\epsilon}, \tag{15}$$

where σ is the surface charge density of the shell. $E_r(a_+)$ denotes the limiting value of E_r as r approaches a from more positive values, and similarly for $E_r(a_-)$. This completes the specification of the boundary conditions.

Finally, we cast the Poisson-Boltzmann equation into dimensionless form. This makes the number of free parameters in the problem obvious and is a convenient form for computation, because the magnitudes of computed quantities are then often close to 1. We use the dimensionless potential $\phi = e_0\Phi/kT$ and a scaled length $\xi = r/a$. Then, substituting Eq. 14 into Eq. 13, multiplying by e_0/kT, and introducing a form for the Laplacian in spherical coordinates (with radial symmetry), we obtain Eq. 1 for the charged-shell model, with the boundary conditions Eqs. 2–5.

The Poisson-Boltzmann equation is only approximate. Long ago, Onsager (1933) argued that it is inconsistent with thermodynamics, especially in the nonlinear regime $\phi \gg 1$. The difficulty arises from the use of

the simple macroscopic electrical potential $z\phi$ to represent the equilibrium energy of an ion, with valence z, in an electrolyte. However, counter-ion concentrations in the vicinity of charged membranes have been measured well into the nonlinear regime (Eisenberg et al., 1979; Bedzyk et al., 1990). The results are in general agreement with the Poisson-Boltzmann equation, if an additional term is added to allow for Stern condensation of ions to the membrane.

The charged-shell model does not include an effect analogous to Stern condensation onto the shell. We do not expect that direct binding of monovalent counter-ions to fixed charges or the channel entrance is important at the low concentrations of interest here. MacKinnon et al. (1989) modeled the effect of surface charges on ion conduction through a K^+ channel and concluded that direct binding of monovalents was not significant below $c_b = 300$ mM. However, this effect could be incorporated into the model following, for example, the method of Dani (1986).

The assumption that local permeant ion concentrations will be in thermodynamic equilibrium with their bulk concentrations is another approximation. The flow of permeant ions through the channel will obviously influence their distribution in the vicinity of the channel entrance. Depletion of permeant ions on the side from which net current is flowing will be associated with an "access resistance" (Läuger, 1976). This effect in particular could be important under the conditions of low ionic strength.

B. Solution of linearized charged-shell model

The nonlinear term $\kappa^2 a^2 \sinh \phi$ in Eq. 1 makes analytical solution difficult or impossible. However, when the potential $\phi < 1$, one has $\sinh \phi \approx \phi$. In this Appendix we solve the resultant linearized equation, using the boundary conditions described below Eq. 1. Physically, we expect these solutions to be accurate when $s < 1$ and, for general s, in the limits $\kappa a \to \infty$ and $\kappa a \to 0$. Strong screening corresponds to $\kappa a \to \infty$ and weak screening to $\kappa a \to 0$. In this last case, nonlinear screening becomes unimportant because few counter-ions are available to screen! Linearizing Eq. 1, we have

$$\frac{d^2}{d\xi^2}\xi\phi = \kappa^2 a^2 \xi\phi, \tag{16}$$

which has a general solution of the form

$$\xi\phi = Ae^{\kappa a\xi} + Be^{-\kappa a\xi}. \tag{17}$$

We first consider separately the problems interior and exterior to the shell. Outside the shell, the condition that $\phi \to 0$ as $r \to \infty$ implies $A = 0$ for the exterior problem. Inside the shell, the condition $\phi'(0) = 0$ implies $B = -A$, as an explicit expansion of ϕ through terms of order $(\kappa a\xi)^2$ will verify. The continuity of ϕ and discontinuity s of ϕ' determine the remaining arbitrary constants, and we obtain the solution

$$\phi(\xi) = \begin{cases} -s\dfrac{\sinh \kappa a\xi}{\kappa a\xi}e^{-\kappa a} & \xi \le 1 \\ -s \sinh \kappa a \dfrac{e^{-\kappa a\xi}}{\kappa a\xi} & \xi \ge 1. \end{cases} \tag{18}$$

In particular, we have for the potentials at the channel entrance and the shell itself

$$\phi(0) = -se^{-\kappa a}, \tag{19}$$

$$\phi(1) = -s\frac{\sinh \kappa a}{\kappa a}e^{-\kappa a}. \tag{20}$$

These formulas have several properties of the numerically computed solution of the full nonlinear equations, which we discuss below. As the bulk ion concentration c_b increases, the Debye length κ^{-1} decreases, and the dimensionless parameter κa grows in proportion to $c_b^{1/2}$. Eq. 19 then implies that the charged-shell contribution to $\phi(0)$ declines fairly rapidly, and c_e, given by Eq. 8, decays to c_b.

In contrast to the entrance potential, the potential at the charged shell, Eq. 20, decreases only with the Debye length ($\kappa^{-1} \propto c_b^{-1/2}$) as bulk ion concentration increases ($\sinh \kappa a \propto e^{\kappa a}$ for κa large). This is qualitatively the same behavior as the surface potential on a sphere, $-s/(1 + \kappa a)$, given by Debye-Hückel theory. As a result, local ion concentrations at the charged shell are much higher than those at the channel entrance when c_b is large. This result is consistent with the numerical solutions given by Fig. 2.

At low ion concentrations $\phi(0)$ is nearly equal to $\phi(1)$. The difference between their two expressions is the factor $\sinh \kappa a/\kappa a$ in Eq. 20; this ratio is nearly equal to 1 when $\kappa a \ll 1$. This result correctly reflects the property that the electrical potential in the interior of the charged shell does not vary greatly under these conditions.

Local ion concentrations computed from the linearized solutions when $s \gg 1$ and at intermediate values of κa are far too great. As c_b increases from zero, c_e may climb very rapidly to a maximum value and then decline again as the exponential decay in Eq. 19 begins to take effect. For example, let $a = 5$ nm and $\zeta = -30$. Then $s = 8.58$ and, according to the linearized theory, c_e attains a maximum value of about 1.25 M when $c_b = 2.3$ mM. However, the corresponding entrance concentration computed numerically from Eq. 1 is only 139 mM. In contrast to the linearized case, entrance ion concentrations computed from the numerical solutions of the nonlinear Boltzmann equation increase monotonically with c_b in every case we have studied.

C. Implementation of numerical method

Numerical solutions of the charged-shell model, Eq. 1, were obtained by the method of shooting (see, for example, Press et al., 1986). This method was used previously by Dani (1986), in his analysis of the Poisson-Boltzmann equation in a vestibule geometry. In this Appendix, we briefly describe some details of its implementation in the charged-shell geometry.

Shooting is a method of solving boundary value problems for ordinary differential equations. We integrated Eq. 1 as an initial value problem from the boundary at $\xi = 0$ and from an exterior boundary, in both cases toward an intermediate fitting point at the charged shell, $\xi = 1$. The two sets of initial conditions were optimized in order to make the potential at the charged shell continuous and to make the derivatives satisfy Eq. 15. Corrections to the initial conditions were calculated using two-dimensional Newton-Raphson iteration. Our computer program adapts code given in *Numerical Recipes* (Press et al., 1986).

In implementing this method, the boundary condition at $\xi = \infty$ cannot be used directly. One way to treat the exterior boundary would be to place it many Debye lengths from the charged shell and specify that the potential go to zero there. The derivative of the potential at the exterior boundary would then be available for optimization. However, the desired value of the derivative at the exterior boundary would itself be very close to zero, and the potential at the fitting point would be extremely sensitive to numerical errors. As an alternative, we placed the exterior boundary only 4 Debye lengths from the charged shell, at $\xi = 1 + 4/\kappa a$. Instead of specifying that the potential go to zero, we required that it be related to its derivative in the same way as the solution to the linearized problem, namely, $\phi' + (\kappa a + \xi^{-1})\phi = 0$. This condition is appropriate so long as $\phi \ll 1$ at the exterior boundary. For the cases explored in this paper, we found $\phi(1 + 4/\kappa a) \le 10^{-2}$.

The interior boundary is singular, reflecting the factor of ξ^{-1} in front of the first derivative in Eq. 1. We integrated away from $\xi = 0$ by expanding the solution in power series. Numerical integration began at $\xi = 0.01$.

D. Dissociation constants of 3B2S models

Consider a symmetrical 3B2S permeation model with uniform binding site and uniform barrier free energies. We assume that only single-ion occupancy is important under the low-ionic-strength conditions of the measurements shown in Fig. 4 *B*. Many results for this case can be derived from the general analysis of single ion rate theory models by Läuger (1973). Schumaker and MacKinnon (1990) give a derivation of the single ion conductance formula specialized to a highly symmetrical model.

Ravindran et al. (1991) and Naranjo and Latorre (1992) give values for dissociation constants $K_S = \exp(E_{site}/kT)$, where E_{site} is the energy of an ion bound at a binding site relative to a standard aqueous solution (usually E_{site}

< 0). Under conditions of low ionic strength, K_S^{-1} is proportional to occupation probability for individual binding sites. For a symmetrical 3B2S single-ion channel, K_S is related to the dissociation constant K_C for the channel itself by $K_C = K_S/2$.

The maximum conductance is also easy to calculate for the symmetrical channels we are considering. Its value is $\gamma_{max} = (z^2e_0^2/kT)b/6$, where b is the frequency of transitions from a binding site across an adjacent barrier (Schumaker and MacKinnon, 1990).

Constraining the 3B2S permeation model of Ravindran et al. (1991) to single-ion occupancy, the appropriate Langmuir parameters are found to be K_C = 1.85 mM and γ_{max} = 14.6 pS. These closely match the fitted values of the Langmuir isotherm to the pH 7.4 rat conductance data in Fig. 4 *B*.

We greatly appreciate helpful conversations with Peter Jordan, Roderick MacKinnon, and Edward Moczydlowski. Roderick MacKinnon reviewed a preliminary version of the manuscript and made several valuable suggestions. We also thank Barry Honig for making the program DELPHI available for our use. Mark Quigley and Walt Sheppard helped us adapt DELPHI to computers at WSU. D. B. C. thanks Christopher Miller (GM-31768) for encouragement and support.

While at Brandeis D. B. C. was supported by a Brittner Fellowship and training grant T32-GM0796. This work was also supported in part by grant FNI 863-1991 to R. L.

REFERENCES

Agnew, W. S., S. R. Levinson, J. S. Brabson, and M. A. Raftery. 1978. Purification of the tetrodotoxin binding component associated with the voltage-sensitive sodium channel from *Electrophorus electricus* electroplax membranes. *Proc. Natl. Acad. Sci. USA.* 76:2602–2610.

Apell, H-J., E. Bamberg, H. Alpes, and P. Läuger. 1977. Formation of ion channels by a negatively charged analog of gramicidin A. *J. Membr. Biol.* 31:171–188.

Apell, H-J., E. Bamberg, and P. Läuger. 1979. Effects of surface charge on the conductance of the gramicidin channel. *Biochim. Biophys. Acta.* 562: 369–378.

Bedzyk, M. J., G. M. Bommarito, M. Caffrey, and T. L. Penner. 1990. Diffuse-double layer at a membrane-aqueous interface measured with x-ray standing waves. *Science (Washington DC).* 248:52–56.

Behrens, M. I., A. Oberhauser, F. Bezanilla, and R. Latorre. 1989. Batrachotoxin-modified sodium channels from squid optic nerve in planar bilayers. *J. Gen. Physiol.* 93:23–41.

Bell, J. E., and C. Miller. 1984. Effects of phospholipid surface charge on ion conduction in the K^+ channel of sarcoplasmic reticulum. *Biophys. J.* 45:279–287.

Cai, M., and P. Jordan. 1990. How does vestibule surface charge affect ion conduction and toxin binding in a sodium channel? *Biophys. J.* 57: 883–891.

Cherbavaz, D. B. 1991. The effect of protein surface charge on batrachotoxin-activated sodium channel function. Ph.D. thesis. Brandeis University.

Correa, A. M., R. Latorre, and F. Bezanilla. 1991. Ion permeation in normal and batrachotoxin-modified Na^+ channels in the squid giant axon. *J. Gen. Physiol.* 97:605–625.

Dani, J. A. 1986. Ion-channel entrances influence permeation. *Biophys. J.* 49:607–618.

Eisenberg, M., T. Gresalfi, T. Riccio, and S. McLaughlin. 1979. Adsorption of monovalent cations to bilayer membranes containing negative phospholipids. *Biochemistry.* 18:5213–5223.

Green, W. N., O. S. Andersen. 1991. Surface charges and ion channel function. *Annu. Rev. Physiol.* 53:341–359.

Hartsel, S. C., and D. S. Cafiso 1986. A test of discreteness-of-charge effects in phospholipid vesicles: measurements using paramagnetic amphiphiles. *Biochemistry.* 25:8214–8219.

James, W. M., and W. S. Agnew. 1987. Multiple oligosaccharide chains in the voltage-sensitive Na channel from *Electrophorus electricus*: evidence for α-2,8-linked polysialic acid. *Biochem. Biophys. Res. Commun.* 148: 817–826.

Jordan, P. C. 1993. Interactions of ions with membrane proteins. *In* Thermodynamics of Membrane Receptors and Channels. M. B. Jackson, editor. CRC Press, Boca Raton. 27–80.

Latorre, R., P. Labarca, and D. Naranjo 1992. Surface charge effects on ion conduction in ion channels. *Methods Enzymol.* 207:471–501.

Läuger, P. 1973. Ion transport through pores: a rate theory analysis. *Biochim. Biophys. Acta.* 311:423–441.

Läuger, P. 1976. Diffusion-limited ion flow through pores. *Biochim. Biophys. Acta.* 455:493–509.

Levitt, D. 1986. Interpretation of biological ion channel flux data—reaction rate versus continuum theory. *Annu. Rev. Biophys. Biophys. Chem.* 15: 29–57.

Mathias, R. T., G. J. Baldo, K. Manivannan, and S. McLaughlin. 1992. Discrete charges on biological membranes. *In* Electrified Interfaces in Physics, Chemistry and Biology. R. Guidelli, editor. Kluwer Academic Publishers, Dordrecht, the Netherlands. 473–490.

MacKinnon, R., R. Latorre, and C. Miller. 1989. Role of surface electrostatics in the operation of a high-conductance Ca^{2+}-activated K^+ channel. *Biochemistry.* 28:8092.

McLaughlin, S. 1977. Electrostatic potentials at membrane-solution interfaces. *Curr. Top. Membr. Transp.* 9:71–144.

Miller, J. A., W. S. Agnew, and S. R. Levinson. 1983. Principal glycopeptide of the tetrodotoxin/saxitoxin binding protein from *Electrophorus electricus:* isolation and partial chemical and physical characterization. *Biochemistry.* 22:462–470.

Moczydlowski, E., and R. Latorre. 1983. Gating kinetics of Ca^{2+}-activated K^+ channels from rat muscle incorporated into planar lipid bilayers. *J. Gen. Physiol.* 82:511–542.

Moczydlowski, E., O. Alvarez, C. Vergara, and R. Latorre. 1985. Effect of phospholipid surface charges on the conductance and gating of a Ca^{2+}-activated K^+ channel in planar lipid bilayers. *J. Membr. Biol.* 83:273–282.

Naranjo, D., and R. Latorre. 1993. Ion conduction substates of the batrachotoxin-modified Na^+ channel from toad skeletal muscle. *Biophys. J.* 64:1038–1050.

Nelson, A. P., and D. McQuarrie. 1975. The effect of discrete charges on the electrical properties of a membrane. I. *J. Theor. Biol.* 55:13–27.

Nicholls, A., and B. Honig. 1991. A rapid finite difference algorithm, utilizing successive over-relaxation to solve the Poisson-Boltzmann equation. *J. Comp. Chem.* 12:435–445.

Onsager, L. 1933. Theories of concentrated electrolytes. *Chem. Rev.* 13: 73–89.

Press, W. H., B. P. Flannery, S. A. Teukolsky, and W. T. Vetterling. 1986. Numerical Recipes. Cambridge University Press, Cambridge.

Ravindran, A., H. Kwiecinski, O. Alvarez, G. Eisenman, and E. Moczydlowski. 1992. Modeling ion permeation through batrachotoxin-modified Na^+ channels from rat skeletal muscle with a multi-ion pore. *Biophys. J.* 61:494–508.

Recio-Pinto, E., W. B. Thornhill, D. S. Duch, S. R. Levinson, and B. W. Urban. 1990. Neuraminidase treatment modifies the function of electroplax sodium channels in planar lipid bilayers. *Neuron.* 5:675–684.

Scheuer, T., L. McHugh, F. Tejedor, and W. Catterall. 1988. Functional properties of neuramidase-treated rat brain sodium channels. *Biophys. J.* 53:541*a*. (Abstr.)

Schumaker, M. F., and R. MacKinnon. 1990. A simple model for multi-ion permeation. *Biophys. J.* 58:975–984.

Terlau, H., S. H. Heinemann, W. Stühmer, M. Pusch, F. Conti, K. Imoto, and S. Numa. 1991. Mapping the site of block by tetrodotoxin and saxitoxin of sodium channel II. *FEBS Lett.* 293:93–96.

Winiski, A. P., A. C. McLaughlin, R. V. McDaniel, M. Eisenberg, and S. McLaughlin. 1986. An experimental test of the discreteness-of-charge effect in positive and negative lipid bilayers. *Biochemistry.* 25: 8206–8214.